FULL PAPERS

Synthesis, Spectroscopy, Crystal Structure Determination, and Quantum Chemical Calculations of BODIPY Dyes with Increasing Conformational Restriction and Concomitant Red-Shifted Visible Absorption and Fluorescence Spectra

Volker Leen,[a] Wenwu Qin,*[b] Wensheng Yang,[b] Jie Cui,[b] Chan Xu,[b] Xiaoliang Tang,[b] Weisheng Liu,[b] Koen Robeyns,[a] Luc Van Meervelt,[a] David Beljonne,[c] Roberto Lazzaroni,[c] Claire Tonnelé,[c] Noël Boens,[a] and Wim Dehaen*[a]

Abstract: Starting from the conformationally unconstrained compound 3,5-di-(2-bromophenoxy)-4,4-difluoro-8-(4-methylphenyl)-4-bora-3a,4a-diaza-s-indacene (**1**), two BODIPY dyes (**2** and **3**) with increasingly rigid conformations were synthesized in outstanding total yields through palladium catalyzed intramolecular benzofuran formation. Restricted bond rotation of the phenoxy fragments leads to dyes **2** and **3**, which absorb and fluoresce more intensely at longer wavelengths relative to the unconstrained dye **1**. Reduction of the conformational flexibility in **2** and **3** leads to significantly higher fluorescence quantum yields compared to those of **1**. X-ray diffraction analysis shows the progressively more extended planarity of the chromophore in line with the increasing conformational restriction in the series **1→2→3**, which explains the larger red shifts of the absorption and emission spectra. These conclusions are confirmed by quantum chemical calculations of the lowest electronic excitations in **1–3** and dyes of related chemical structures. The effect of the molecular structure on the visible absorption and fluorescence emission properties of **1–3** has been examined as a function of solvent by means of the new, generalized treatment of the solvent effect (*J. Phys. Chem. B* **2009**, *113*, 5951–5960). Solvent polarizability is the primary factor responsible for the small solvent-dependent shifts of the visible absorption and fluorescence emission bands of these dyes.

Keywords: BODIPY · conformational mobility · crystal structure · fluorescent dyes · solvent effect

Introduction

Since the appearance of difluoroboron dipyrromethene[1,2] (or BODIPY[3]) dyes in the late 1960s, considerable effort has been put in the conversion of their favorable spectroscopic properties to longer wavelengths. The search for bright fluorophores that absorb and emit in the red visible (Vis) to the near infrared (NIR) spectral range continues

[a] Dr. V. Leen, Dr. K. Robeyns, Prof. L. Van Meervelt, Prof. N. Boens, Prof. W. Dehaen
Department of Chemistry
Katholieke Universiteit Leuven
Celestijnenlaan 200f—bus 02404, 3001 Leuven (Belgium)
Fax: (+32) 16-327990
E-mail: Wim.Dehaen@chem.kuleuven.be

[b] Prof. Dr. W. Qin, W. Yang, J. Cui, C. Xu, Dr. X. Tang, Prof. Dr. W. Liu
Key Laboratory of Nonferrous Metal Chemistry and
Resources Utilization of Gansu Province
and State Key Laboratory of Applied Organic Chemistry
College of Chemistry and Chemical Engineering
Lanzhou University
Lanzhou 730000 (China)
Fax: (+86) 931-8912582
E-mail: qinww@lzu.edu.cn

[c] Prof. Dr. D. Beljonne, Prof. Dr. R. Lazzaroni, C. Tonnelé
Laboratory for Chemistry of Novel Materials
Université de Mons
Place du Parc 20, 7000 Mons (Belgium)

View this journal online at wileyonlinelibrary.com
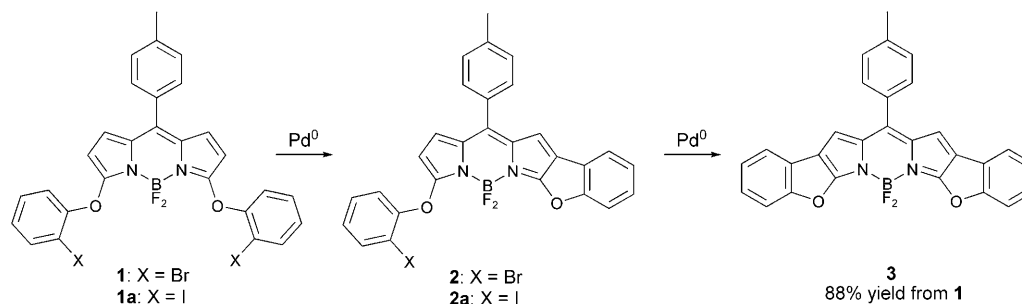
Scheme 1. Transition metal catalyzed benzofuran formation.

ceaselessly. Stable dyes with sharp absorption and fluorescence emission bands in the red or NIR region of the spectrum, combined with high molar absorption coefficients $\varepsilon(\lambda)$ and high fluorescence quantum yields Φ_f, may find extensive use in many different fields, such as optical engineering, analytical chemistry, biological in vivo imaging and sensing applications, and materials science.[3, 4]

In recent years, a substantial number of research publications have focused on the syntheses, functionalization reactions, and spectroscopic/photophysical properties of 4,4-difluoro-4-bora-3a,4a-diaza-s-indacene dyes. Extension of the conjugated system is the most widely used method to obtain BODIPY dyes with spectra shifted to longer wavelengths.[2] Conveniently, this can be established by substitution of the BODIPY core with aromatic groups.[5, 6] 3,5-Diaryl substituted BODIPY dyes can show a bathochromic shift of over 100 nm, but generally have low to moderately high fluorescence quantum yields Φ_f, owing to nonradiative decay through rotational relaxation of the aromatic substituents. The introduction of alkenyl substituents produces even larger bathochromic shifts and the rigidity of the double bond generally results in higher Φ_f values.[6–8] Alkyne substitution at the 3(,5)-position(s) produces interesting BODIPY fluorophores with high quantum yields and large red shifts.[6, 9]

Annulation, that is, the building of a ring onto some starting molecule, can be used to extend the ring system and reduce the nonradiative decay through rotational relaxation and hence to enhance fluorescence. Building of heterocyclic rings onto the aromatic rings attached to the BODIPY core can even lead to NIR emitting dyes. Burgess et al. described conformationally constrained, aryl-substituted BODIPY dyes.[10] Ono et al. reported the synthesis and optical properties of BODIPY dyes fused with rigid bicyclo rings.[11] Goeb and Ziessel prepared benzo fused BODIPY dyes substituted with 3,5-dithienyl groups and with alkynylaryl fragments at the boron center.[12] A series of bright fluorophores named Keio Fluors, based on BODIPY, were reported by Suzuki et al.[13, 14] Shen, You, Rurack, and co-workers described phenanthrene-fused[15] and dihydronaphthalene-fused[16] BODIPY dyes. The preparation of all these reported, rigid BODIPY dyes required lengthy multi-step syntheses of the ring-fused pyrroles as starting materials. Intrigued by these reports on fluorescent dyes with extended conjugation and

restricted bond rotations, we designed a convenient and highly efficient two-step synthetic route to BODIPY derivatives fused with rigid benzofuran units. The advantages of our synthetic strategy are two-fold: i) this synthesis eliminates the tedious preparation of ring-fused pyrroles, ii) through this sequential ring formation reaction, a nonsymmetric dye is easily accessible.

In the present work, we prepared three 4,4-difluoro-4-bora-3a,4a-diaza-s-indacene dyes (**1–3**, Scheme 1) with increasingly rigid conformations caused by benzofuran ring formation. We investigated their spectroscopic and photophysical characteristics in a large number of solvents by UV/Vis spectrophotometry and steady-state fluorescence spectroscopy. These experiments allowed us to determine the wavelengths of the spectral maxima [$\lambda_{abs}(\max)$, $\lambda_{ex}(\max)$, $\lambda_{em}(\max)$], the full width at half height of the maximum of the absorption (fwhm$_{abs}$) and fluorescence emission (fwhm$_{em}$) bands, the Stokes shifts ($\Delta\bar{\nu}$), and the fluorescence quantum yields (Φ_f). We used single- and multi-parameter expressions to describe the solvent effect on the position of the spectral maxima and Stokes shifts of **1–3**. In addition, X-ray diffraction analysis of **1–3** was performed and revealed an increasingly more extensive planarity of the chromophore in line with reduction of conformational flexibility. Finally, quantum chemical calculations were performed to understand the spectroscopic properties of **1–3** and related, previously described ring-fused BODIPY dyes.

Results and Discussion

Synthesis

As reported in our earlier work,[17–19] 3,5-dichlorinated BODIPY dyes (such as **4**, Scheme 2) can be substituted efficiently by a variety of nucleophiles. In a previous report, we described the synthesis of compound **1** (with o-bromophenoxy groups at the 3,5-positions of BODIPY) (Scheme 2).[20] Nucleophilic aromatic substitution of 3,5-dichloro-BODIPY **4** with 2-bromophenol and 2-iodophenol takes place readily and in near quantitative yield, furnishing the desired starting compounds **1** and **1a** in gram scale.

Proper placement of a halogen (X = Br or I) atom on the phenyl ring could make the system susceptible to benzofuran ring formation. Indicative of the plausible reactivity of
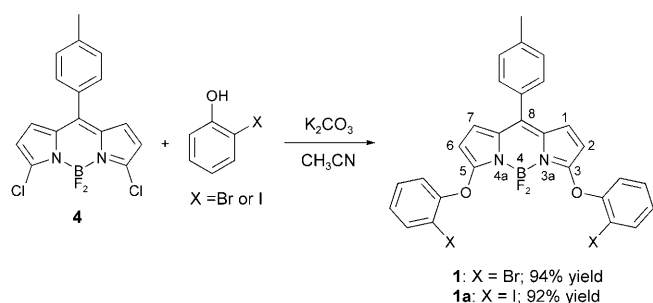
Scheme 2. Nucleophilic substitution of dichloro-BODIPY **4** with *ortho*-halogen phenol nucleophiles. The numbering of the BODIPY core is also indicated.

the 2,6-positions of BODIPY in palladium chemistry, is its use for Heck-type reactions described by Burgess et al.[21] This transition metal catalyzed oxidative ring formation has found widespread use in the synthesis of heteroaromatic systems.[22] In these reactions, the metal of choice is mostly palladium.

Initial experiments with Pd⁰ sources proved the viability of our premise: the closed products were being formed after prolonged heating (7 days) and in low yield. Often these reactions are carried out in polar solvents, like *N,N*-dimethylformamide (DMF), *N,N*-dimethylacetamide (DMA), or *N*-methylpyrrolidone (NMP), to increase the reaction rate. Although a fast reaction was observed in these solvents, the products had limited stability under these conditions. As optimized reaction conditions, we used Pd[II] precatalysts and the long reaction times could be reduced to two days (Table 1). Even with microwave irradiation (entry 10, MW), the reaction still took 8 h to go to completion. This microwave procedure led to the ring-closed product **3** in excellent yield. Interestingly, stopping the reaction before completion allowed us to isolate the intermediate BODIPY dye **2**. There is no significant difference in reactivity between the first ring formation and the second: compound **2** was separated in 32% yield from a mixture of starting material **1** and dye **3**. The use of a nickel catalyst under similar conditions did not result in the desired ring formation. Also, the use of 2-iodophenol instead of 2-bromophenol did not produce drastic changes. As expected, reactions were faster when using iodinated dye **1a**, and the isolated yield was slightly higher.

Crystallographic Structure

As shown in Figure 1, the boron center of **2** adopts a tetrahedral configuration with bond angles of $\approx 110°$ and bond distances of 1.38 Å (B−F) and 1.55–1.56 Å (B−N). In the BODIPY ring system, the two planar pyrrole subunits and the boron atom constitute a rigid plane, in which the maximum deviation of non-hydrogen atoms is 0.024 Å. The two fluorine atoms are equidistant above and under the mean plane of the BODIPY core, and the F-B-F plane is almost
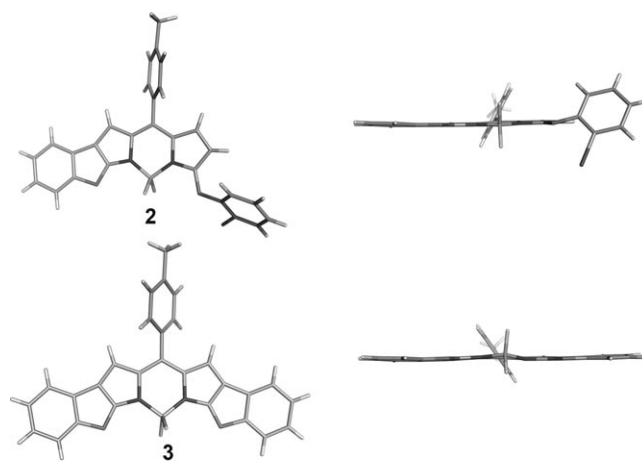

Figure 1. Stick representation of compound **2** (top) and compound **3** (bottom). To illustrate the planarity of the ring systems a bottom view is placed at the right. Created with PyMol, (DeLano, W.L. The PyMOL Molecular Graphics System (2002) from http://www.pymol.org).

perpendicular (89.9°) to the plane of the ring system. The tolyl group at the *meso*-position makes an angle of 62.09° with the BODIPY plane, which is in the range of most BODIPY derivatives (40.3–90°), but is smaller than the average value of 74.5° found in the CSD.[23] A remarkable structural feature is that all of the atoms in the benzofuran fragment also lie in the BODIPY plane, the deviation is within 0.054–0.271 Å. In addition, the 2-bromophenoxy substituent is inclined relative to

Table 1. Reaction conditions of transition metal catalyzed annulation.

Catalyst	Solvent	Ligand	Base	t	T [°C])	Yield [%][a]
[Pd(PPh₃)₄]	DMF	P(Ph)₃	K₂CO₃	18 h	RT	0
[Pd(OAc)₂]	DMF	P(Ph)₃	K₂CO₃	2 h	100	37
[Pd₂(dba)₃]	DMF	dba	K₂CO₃	4 h	100	16
[Pd₂(dba)₃]	xylene[d]	P(furyl)₃	Na₂CO₃	48 h	140	60
[Pd(PPh₃)₄]	dioxane	P(Ph)₃	K₂CO₃	96 h	100	32
[Pd(OAc)₂]	DMF	Bu₄NCl	K₂CO₃	12 h	80	0
[Pd(OAc)₂]	toluene	P(Ph)₃	KOAc	48 h	110	35
[Pd(OAc)₂]	toluene	P(OPh)₃	K₂CO₃	48 h	110	23
[Pd(OAc)₂]	toluene	DPPE	K₂CO₃	72 h	110	55
[Pd(OAc)₂]	toluene	P(Ph)₃	K₂CO₃	8 h (MW)[c]	130	88
[Pd(OAc)₂]	toluene	P(Ph)₃	K₂CO₃	48 h	110	69
[Pd(OAc)₂]	toluene	P(Ph)₃	K₂CO₃	36 h	110	74[b]
[Ni(dppp)]	xylene[d]	DPPP	K₂CO₃	96 h	120	0

[a] Yield of isolated product of **3** starting from a reaction with 0.1 mmol **1**. [b] Yield of isolated product of **3** starting from 0.1 mmol of iodinated compound **1a**. [c] Irradiated at 150 W and 130 °C. [d] A mixture of xylenes is used. dba = dibenzylideneacetone, DPPE = 1,2-bis(diphenylphosphino)ethane, DPPP = 1,3-bis(diphenylphosphino)propane.

the BODIPY plane, and the dihedral angle between both is 58.80°.

For dye **3** (Figure 1), the entire aromatic system is flat: the deviation from planarity for the boron atom, when considering the entire aromatic system, is 0.19 Å. The *p*-tolyl group makes an angle of 55.4° with the BODIPY system.

The structure of **1** was confirmed by X-ray analysis, however the crystals diffract poorly and the structure will not be discussed here. The ORTEP representation of dye **1** (as well as **2** and **3**) is shown in Figure S1 in the Supporting Information for reference purposes.

Spectroscopic Properties

Dyes **1**–**3** are strongly colored solids with a metallic luster that form intensely colored solutions with a bright fluorescence when irradiated (Figure S2 in the Supporting Information).

The UV/Vis absorption and fluorescence emission spectra of **1** dissolved in a limited number of solvents have been reported before.[20] The number of solvents used in the analysis of the solvatochromism of **1** was extended to twenty in the current investigation. We also used twenty solvents in the analysis of the solvatochromism of **2** and **3**.

Compound **1** displays the typical absorption features of classic BODIPY dyes in all solvents studied (Figure 2): that is, a narrow absorption band with a maximum in the $\lambda = 511$–518 nm range, irrespective of the solvent employed. This absorption band is assigned to the $S_1 \leftarrow S_0$ transition, while an additional, considerably weaker, broad absorption band, observed at the short wavelength side, is attributed to the $S_2 \leftarrow S_0$ transition.

The main absorption band of **1** is hardly affected by solvent polarity: The maximum being slightly blue-shifted when the solvent is changed from toluene ($\lambda = 518$ nm) to acetonitrile or diethyl ether ($\lambda = 511$ nm), which is consistent with the general behavior of BODIPY chromophores.[24]

Derivative **1** also shows the typical emission features of BODIPY, these are, a narrow, lightly Stokes-shifted band of mirror image shape, and fluorescence bands that are blue-shifted with decreasing solvent polarizability (from $\lambda = 537$ nm in CCl$_4$ to $\lambda = 528$ nm in methanol). The fluorescence quantum yields Φ_f are 0.27–0.71. Compiled in Table 2 are the spectroscopic and photophysical data of **1** as a function of solvent.
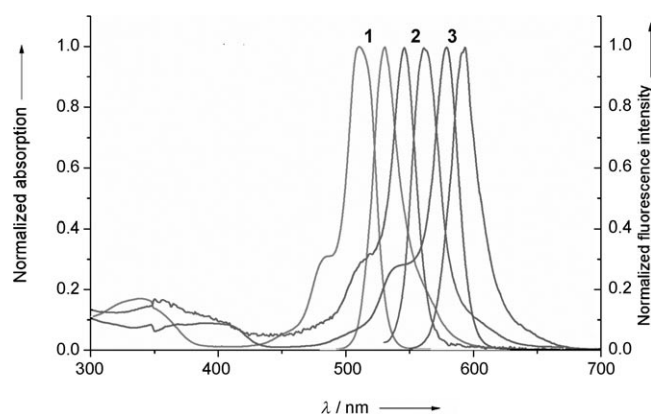

Figure 2. Normalized absorption and fluorescence emission profiles of **1**–**3** in diethyl ether.

Table 2. Spectroscopic/photophysical properties of **1** in several solvents. The solvents are numbered according to increasing refractive index n.

	Solvent	λ_{abs}(max) [nm]	λ_{em}(max) [nm]	$\Delta\bar{\nu}$ [cm^{-1}]	fwhm$_{abs}$ [cm^{-1}]	fwhm$_{em}$ [cm^{-1}]	Φ_f
1	methanol	512	528	592	726	926	0.41 ± 0.03
2	acetonitrile	511	529	666	806	956	0.29 ± 0.01
3	diethyl ether	511	530	702	992	848	0.38 ± 0.01
4	acetone	512	530	663	766	919	0.29 ± 0.02
5	ethyl acetate	513	531	661	724	990	0.27 ± 0.01
6	2-propanol	514	531	623	721	848	0.58 ± 0.01
7	butanenitrile	513	532	696	806	946	0.38 ± 0.02
8	dibutyl ether	513	532	696	909	842	0.48 ± 0.02
9	1-butanol	515	533	656	718	845	0.61 ± 0.04
10	THF	515	532	620	757	979	0.29 ± 0.02
11	1-pentanol	516	533	618	715	842	0.64 ± 0.05
12	1,4-dioxane	515	534	691	754	839	0.47 ± 0.02
13	dichloromethane	516	533	618	754	876	0.44 ± 0.02
14	cyclohexane	516	532	583	676	949	0.48 ± 0.03
15	DMF	515	534	691	794	975	0.29 ± 0.02
16	1-decanol	517	533	581	712	805	0.71 ± 0.02
17	chloroform	518	535	613	710	833	0.63 ± 0.01
18	tetrachloromethane	518	537	683	671	833	0.58 ± 0.03
19	DMSO	516	536	723	790	902	0.38 ± 0.03
20	toluene	518	536	648	710	902	0.47 ± 0.01

The absorption and fluorescence emission spectra of **2** and **3** (Figure 2; Figure S3 and S4 in the Supporting Information) are of similar shape as those of similar, previously described difluoroboron dipyrromethene dyes.[24] Introduction of the benzofuran ring in **2** causes a large bathochromic (≈ 30 nm) shift in both the absorption [λ_{abs}(max)] and emission [λ_{em}(max)] maxima compared to **1** (Table 3). The absorption and emission maxima of the most rigid structure **3** are further red-shifted by approximately 30 nm compared with **2** (Table 4). The progressively more extended planarity of the chromophore in the series **1**→**2**→**3** accounts for the increasing bathochromic shifts of λ_{abs}(max) and λ_{em}(max). The fact that the absorption band positions of **1**–**3** do not show any particular trend as a function of solvent polarity suggests that the absorbing state of the dyes is weakly dipolar.

FULL PAPERS

Table 3. Spectroscopic/photophysical properties of **2** in several solvents. The solvents are numbered according to increasing refractive index n.

	Solvent	λ_{abs}(max) [nm]	λ_{em}(max) [nm]	$\Delta\bar{\nu}$ [cm^{-1}]	fwhm$_{abs}$ [cm^{-1}]	fwhm$_{em}$ [cm^{-1}]	Φ_f
1	methanol	544	562	589	918	821	0.57 ± 0.02
2	acetonitrile	544	563	620	954	785	0.59 ± 0.04
3	diethyl ether	546	563	553	776	758	0.62 ± 0.08
4	acetone	544	563	620	918	788	0.57 ± 0.02
5	ethyl acetate	547	562	488	844	755	0.63 ± 0.01
6	2-propanol	547	563	520	805	725	0.64 ± 0.05
7	butanenitrile	544	564	652	990	845	0.70 ± 0.01
8	dibutyl ether	549	565	516	733	722	0.57 ± 0.01
9	1-butanol	549	565	516	802	722	0.56 ± 0.02
10	THF	547	563	520	873	720	0.50 ± 0.01
11	1-pentanol	549	565	516	800	750	0.71 ± 0.07
12	1,4-dioxane	549	565	516	800	717	0.55 ± 0.03
13	dichloromethane	550	566	514	831	747	0.59 ± 0.01
14	cyclohexane	551	564	418	661	662	0.69 ± 0.04
15	DMF	547	567	645	1011	809	0.42 ± 0.02
16	1-decanol	551	566	481	794	717	0.78 ± 0.01
17	chloroform	553	567	446	791	682	0.58 ± 0.04
18	tetrachloromethane	553	567	446	656	714	0.63 ± 0.02
19	DMSO	549	567	578	1003	742	0.53 ± 0.15
20	toluene	553	569	508	788	742	0.48 ± 0.01

Table 4. Spectroscopic/photophysical properties of **3** in several solvents. The solvents are numbered according to increasing refractive index n.

	Solvent	λ_{abs}(max) [nm]	λ_{em}(max) [nm]	$\Delta\bar{\nu}$ [cm^{-1}]	fwhm$_{abs}$ [cm^{-1}]	fwhm$_{em}$ [cm^{-1}]	Φ_f
1	methanol	576	590	412	787	767	0.63 ± 0.03
2	acetonitrile	578	592	409	876	767	0.58 ± 0.02
3	diethyl ether	578	593	438	687	710	0.69 ± 0.03
4	acetone	577	593	468	816	824	0.58 ± 0.04
5	ethyl acetate	579	593	408	750	794	0.61 ± 0.05
6	2-propanol	580	593	378	716	764	0.62 ± 0.06
7	butanenitrile	579	593	408	842	875	0.64 ± 0.01
8	dibutyl ether	582	594	347	654	791	0.77 ± 0.07
9	1-butanol	582	594	347	742	789	0.58 ± 0.17
10	THF	580	595	435	745	786	0.56 ± 0.08
11	1-pentanol	582	596	404	711	786	0.62 ± 0.05
12	1,4-dioxane	583	596	374	768	768	0.62 ± 0.14
13	dichloromethane	583	597	402	740	807	0.63 ± 0.07
14	cyclohexane	583	593	289	589	735	0.65 ± 0.06
15	DMF	580	597	491	836	866	0.51 ± 0.05
16	1-decanol	584	597	373	676	783	0.65 ± 0.05
17	chloroform	586	599	370	732	805	0.63 ± 0.19
18	tetrachloromethane	588	598	284	641	754	0.59 ± 0.12
19	DMSO	587	599	341	1346	890	0.75 ± 0.01
20	toluene	587	602	424	699	799	0.58 ± 0.08

Excitation by light yields fluorescence emission spectra with mirror image shape of the absorption spectra. The Stokes shifts $\Delta\bar{\nu}$ are small for **1**–**3** and decrease with diminishing conformational mobility ($\bar{\nu} = 651 \pm 43$ cm^{-1} for **1**, $\bar{\nu} = 533 \pm 66$ cm^{-1} for **2**, and 390 ± 52 cm^{-1} for **3**) (Tables 2–4). The fluorescence excitation spectra of **1**–**3** match the absorption spectra in all cases and, moreover, λ_{ex}(max) = λ_{abs}(max). The observation that the emission band positions of **1**–**3** do not exhibit any distinct trend as a function of solvent polarity implies that emission occurs from the weakly dipolar, relaxed Franck–Condon excited state of the dyes.

The increasingly restricted bond rotation in the ring-fused systems **2** and **3** explains the noticeably higher quantum yields Φ_f of **3** ($\Phi_f \geq 0.5$ in all 20 solvents studied) and **2** ($\Phi_f \geq 0.5$ in 18 out of 20 solvents) compared to those of **1** ($\Phi_f \geq 0.5$ in 6 out of 20 solvents).

The molar absorption coefficients ε_{max} of **1**–**3** at the absorption maximum λ_{abs}(max) were determined in toluene, ethyl acetate, and methanol (Table 5). The corresponding values of the oscillator strength f calculated according to Equation (1),[4] in which n is the solvent index of refraction and ν is the wavenumber (in cm^{-1}), are also compiled in Table 5.

$$f = \frac{4.32 \times 10^{-9}}{n} \int \varepsilon(\bar{\nu}) d\bar{\nu} \qquad (1)$$

Progressive reduction of the flexibility of the chromophore is reflected by the considerably higher ε_{max}, f, and Φ_f values. The brightness, defined as the product of the molar absorption coefficient $\varepsilon(\lambda)$ at the excitation wavelength λ and the fluorescence quantum yield [$\varepsilon(\lambda) \times \Phi_f$],[25] intensifies considerably by restricting the conformational flexibility. The maximum values of the brightness [i.e., for $\varepsilon(\lambda) = \varepsilon_{max}$ at λ_{abs}(max)] for **1**–**3** in toluene, ethyl acetate, and methanol are given in Table 5.

The average absorption and emission spectral bandwidths of **1**–**3** are quite narrow [fwhm$_{abs}$ = $(7.6 \pm 0.8) \times 10^2$ cm^{-1} for **1**, $(8.4 \pm 1.0) \times 10^2$ cm^{-1} for **2**, and $(7.7 \pm 1.5) \times 10^2$ cm^{-1} for **3**; fwhm$_{em}$ = $(9 \pm 6) \times 10^2$ cm^{-1} for **1**, $(7.6 \pm 0.5) \times 10^2$ cm^{-1} for **2**, and $(7.9 \pm 0.4) \times 10^2$ cm^{-1} for **3**]. Increasing the rigidity of the systems **2** and **3**—by benzofuran formation and by increasing the planarity of the chromophore—diminishes the degrees of vibrational freedom relative to **1**.

These spectral/photophysical properties can be compared to those of conformationally restricted BODIPY dyes published in the literature (Table 6).[10–14, 16] The symmetric, constrained dye **5** (Scheme 3) of Burgess and co-workers[10] with 2,6-dioxy benzofuran rings should be contrasted to com-

Table 5. Spectroscopic/photophysical properties of **1–3**.

Dye	Solvent	λ_{em}(max) [nm]	ε_{max} [L mol^{-1} cm^{-1}]	f	Φ_f	Max. brightness [L mol^{-1} cm^{-1}]
1	MeOH	512	$(42\pm3)\times10^3$	0.307	0.41	17220
	AcOEt	513	$(45\pm4)\times10^3$	0.226	0.27	12150
	toluene	518	$(35\pm2)\times10^3$	0.248	0.47	16450
2	MeOH	544	$(69\pm6)\times10^3$	0.362	0.57	39330
	AcOEt	547	$(72\pm4)\times10^3$	0.359	0.63	45360
	toluene	553	$(42\pm2)\times10^3$	0.390	0.48	20160
3	MeOH	576	$(126\pm6)\times10^3$	1.145	0.63	79380
	AcOEt	579	$(126\pm7)\times10^3$	0.744	0.61	76860
	toluene	587	$(155\pm4)\times10^3$	0.802	0.58	89900

Table 6. Spectroscopic/photophysical properties of (ring-fused) BODIPY dyes from the literature discussed here.
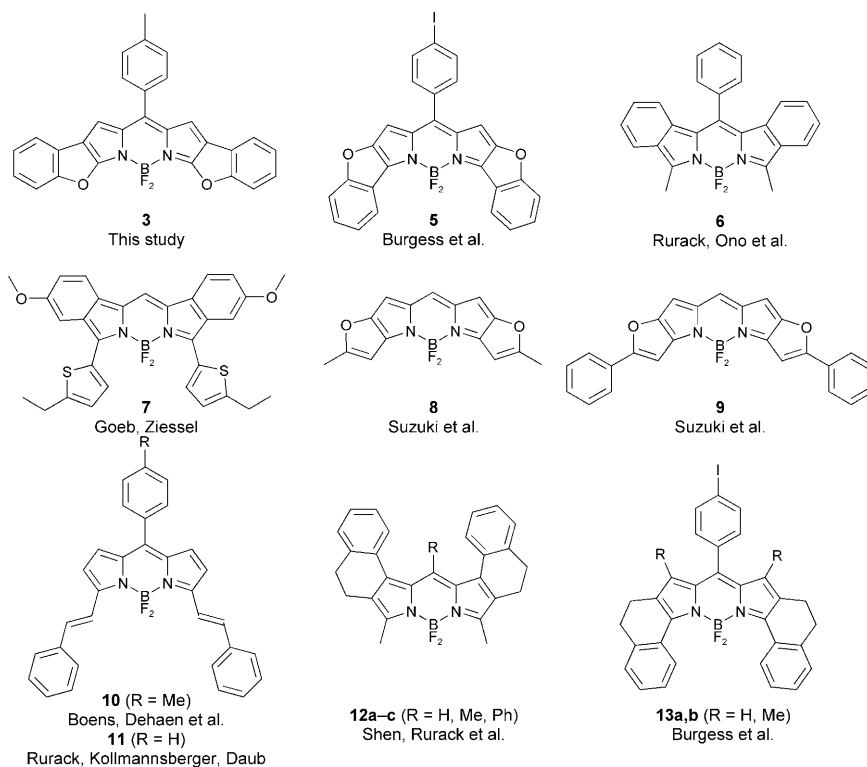
Dye	λ_{abs}(max) [nm]	λ_{em}(max) [nm]	$\Delta\bar{\nu}^{[a]}$ [cm^{-1}]	ε_{max} [L mol^{-1} cm^{-1}]	Φ_f	Solvent	Reference
3	587	602	424	155000	0.58	toluene	this study
5	637	647	243	151000	0.34	CHCl$_3$	[10]
6	600	609	246	[c]	0.99	THF	[11b]
7	727	780	936	90000	0.20	CH$_2$Cl$_2$	[12]
8	579	583	118	202000	0.96	CHCl$_3$	[13,14]
9	652	661	209	314000	0.90	CHCl$_3$	[14]
10	630	642	297	138000$^{[b]}$	0.96	cyclohexane	[6]
11	633	646	318	[c]	0.83	THF	[7]
12a (R=H)	562	569	219	[c]	0.55	THF	[16]
12b (R=Me)	562	599	1099	[c]	0.44	THF	[16]
12c (R=Ph)	573	609	1032	[c]	0.23	THF	[16]
13a (R=H)	634	647	317	126250	0.38	MeOH	[10]
13b (R=Me)	619	629	257	145750	0.72	MeOH	[10]

[a] $\Delta\bar{\nu}$ is calculated from reported λ_{abs}(max) and λ_{em}(max) according to $\Delta\bar{\nu} = 1/\lambda_{abs}(\text{max}) - 1/\lambda_{em}(\text{max})$.
[b] ε_{max} value determined in current study. [c] Not available.

pound **3** with 3,6-dioxy benzofuran rings. The most striking difference between these two dyes is the larger red shifts of λ_{abs}(max) and λ_{em}(max) for dye **5** which absorbs and emits light ≈50 nm more to the red relative to dye **3**. This large difference reflects the improved conjugation of the 2,6-dioxy derivatives compared to the new 3,5-dioxy dyes. The benzo-fused compounds **6** and **7** also have bathochromically shifted λ_{abs}-(max) and λ_{em}(max) relative to **3**. BODIPY **7** has a low Φ_f value, owing to the rotational mobility of the 3,5-dithienyl fragments. The Keio Fluors **8** and **9** of Suzuki et al.[13,14] (with 2,6-dioxy furan rings as in **5**, Scheme 3) have extremely high ε_{max} compared to **3**, **5**, and **7**. The Stokes shifts $\Delta\bar{\nu}$ of **8** and **9** are very small. λ_{abs}(max) and

λ_{em}(max) of **8** (with a single methyl substituent on each furan ring) are slightly blue-shifted relative to those of **3** (with benzofuran rings). Conversely, λ_{abs}(max) and λ_{em}(max) of **9** are located over 650 nm. Dye **9** can be regarded as a 3,5-distyryl substituted BODIPY (such as **10–11**)[6–8] with oxygen atom bridge linkers that preclude free rotation of the ethenyl fragments. The absence of a *meso*-substituent and hence limited conformational flexibility in **8** and **9** leads to very high quantum yields Φ_f. Fusion of dihydronaphthalene groups (with their 1,2-positions) to the 1,2- and 6,7-positions of the BODIPY core (compounds **12a–c**)[16] and to the 2,3- and 5,6-positions (compounds **13a,b**)[10] leads to dyes with red-shifted absorption and fluorescence emission maxima comparable to classic difluoroboron dipyrromethenes. Compounds **13** have more bathochromically shifted spectra than **12**, indicative of a more efficient delocalization in **13**. The decreasing Φ_f values in **12a–c** are in line with the increasing conformational mobility of the *meso*-substituents (H, Me, and Ph). The higher Φ_f value of **13b** in comparison to **13a** arises from the restricted rotational freedom of the 8-substituent imposed by methyl groups at

Scheme 3. Chemical structures of (ring-fused) BODIPY dyes from the literature discussed here.

3 This study
5 Burgess et al.
6 Rurack, Ono et al.
7 Goeb, Ziessel
8 Suzuki et al.
9 Suzuki et al.
10 (R = Me) Boens, Dehaen et al.
11 (R = H) Rurack, Kollmannsberger, Daub
12a–c (R = H, Me, Ph) Shen, Rurack et al.
13a,b (R = H, Me) Burgess et al.

the 1,7-positions. To understand all these experimental observations on ring-fused BODIPY compounds, we performed quantum chemical calculations, which are reported in the next section.

Quantum Chemical Calculations

All dyes studied have a ring-fused BODIPY core. For all compounds investigated, ground-state geometry optimization was first performed at the semi-empirical AM1 level. These geometries were subsequently used as input for excited-state calculations at the AM1/SCI level (in the gas phase). The main goal of the theoretical work is to unravel the relationships between the nature and position of the substituents grafted on the BODIPY core and the resulting spectral properties, namely excitation energy and optical absorption cross-section.

Compounds 1–3

To understand the effect of conformational constraints on the optical properties of BODIPY dyes, we performed calculations on molecules 1–3. Starting from 1, the rigidity of the structure has been increased by the introduction of benzofuran rings instead of bromophenoxy groups (1→2→3, see Figure 1). The results of the AM1/SCI calculations are presented in Table 7.

For 1, the HOMO has no weight on the substituents (bromophenoxy rings). If the bromophenoxy groups of 1 are replaced by either one or two benzofuran rings in 2 and 3, respectively, the HOMO shows significant contributions on the substituent moiety thereby explaining the predicted and measured bathochromic and hyperchromic shifts.

Compounds 3 and 5

It is instructive to compare 3 and 5 as these only differ by the position of the benzofuran rings on the BODIPY core: Compound 3 presents 3,5-dioxy benzofuran rings whereas 5 features 2,6-dioxy benzofuran rings (see Scheme 3).

Experimentally, it has been found that 5 was more red-shifted than 3, reflecting its improved conjugation. The theoretical results confirm this observation (Table 7).

Looking at the transition wavelengths (Table 7), we find $\lambda_{abs}(max) = 562$ nm for 3, which is ≈ 24 nm less than the experimental result. In the case of 5, we find a bigger difference with a transition at $\lambda = 599$ nm, approximately 38 nm less than the experimental one. Again, although the theoretical values of the absorption maxima and of the spectral shifts are underestimated for both compounds, the qualitative trend is nicely reproduced by the calculations, with 5 showing a calculated bathochromic shift of ≈ 37 nm (≈ 0.14 eV) compared to 3 (against the experimental value of ≈ 50 nm).

When comparing the frontier orbitals, a major visible difference can be noticed for the LUMO: in 3, the LUMO has a vanishingly small weight on the benzofuran rings, while these contribute significantly to the LUMO wavefunction in 5. This is confirmed by the computed transition densities (that provide a local map for the transition dipole and the excited-state localization) for the lowest electronic excitation (Figure 3). The transition is
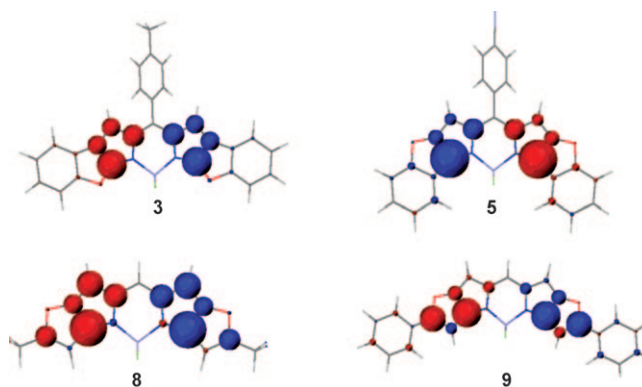
Table 7. Calculated (AM1/SCI) (left) and measured (right) photophysical properties of compounds 1–3, 5, 8–10. To convert the theoretical value of the oscillator strength f (for the gas phase) to values in a solvent with refractive index n, one has to multiply the theoretical f value by $n\left(\frac{n^2+2}{3}\right)^2$.[26]

| | theoretical values (in the gas phase) | | | experimental values | | |
	Transition energy [eV]	Transition wavelength [nm]	Oscillator strength f	Transition energy [eV]	Transition wavelength [nm]	Oscillator strength f
1	2.382	521	0.7515	2.396[a]	518[a]	0.248[a]
2	2.303	538	0.8525	2.245[a]	553[a]	0.390[a]
3	2.206	562	1.0182	2.114[a]	587[a]	0.802[a]
5	2.069	599	0.7912	1.949[b]	637[b]	–
8	2.152	576	0.8544	2.144[b]	579[b]	–
9	2.023	613	1.2316	1.904[b]	652[b]	–
10	2.090	593	0.8995	1.933[c]	642[c]	–

[a] Data in toluene. [b] Data in chloroform. [c] Data in cyclohexane.

The increase in rigidity leads to a bathochromic shift of $\lambda_{abs}(max)$: there is a red shift of ≈ 18 nm (≈ 0.08 eV) when one bromophenoxy group is replaced by a benzofuran ring (in 2). If a second benzofuran ring is introduced (in 3), the bathochromic shift reaches ≈ 24 nm (≈ 0.10 eV) in comparison to 2. The calculations reproduce well the observed spectral shifts, even though the AM1/SCI values are systematically underestimated (see Table 7).

The experimental oscillator strengths, f, extracted from Equation (1), are in line with our theoretical findings: the oscillator strength f increases when the 3,5-substituents are frozen in a more rigid structure, as a result of the extended π delocalization.

Differences between the frontier orbitals of the three compounds are only noticeable in the case of the HOMO.

Figure 3. Transition densities of compounds 3, 5, 8, and 9.

almost completely localized on the BODIPY core in **3**, yet one can see small but non- negligible contributions on the benzofuran rings in **5**, consistent with the extended conjugation. In a simple valence bond picture, the phenyl units in **5** are connected to the central pyrrole rings of the BODIPY core in 'N-α' positions, while they are grafted in 'N-β' positions for **3**, thereby explaining the more efficient delocalization in **5**.

Compounds 8–10

Compounds **8** and **9** differ by the substituent on the furan rings, whereas **9** and **10** are both 3,5-distyryl compounds but **9** is conformationally restricted through *O*-linked bridges. From the spectroscopic data above, it has been found that **9** presents a larger red shift compared to **8** and **10**.

The theoretical λ_{abs}(max) (Table 7) obtained for **8** is in good agreement with the experimental value (underestimated by only ≈3 nm). For **9** and **10**, the computed transition wavelengths are underestimated by a larger amount, of about 40 nm, compared to the experimental results, $\lambda = 652$ and 630 nm, respectively. However, both experimental and theoretical results follow the same tendency and show that preventing rotation by the presence of *O*-linked bridges is an efficient way to increase the oscillator strength.

We can first compare the frontier orbitals of **8** and **10** to disentangle the influence of the presence of *O*-linked bridges. There are no obvious differences neither between the HOMO and LUMO orbitals of the two compounds nor in terms of the transition densities (not shown). It thus appears that extending the conjugation from **8** to **10** through substitutions at the 3,5 positions of the BODIPY core is not very effective in raising the oscillator strength and/or in lowering the excitation energy. We attribute this to the fact that the extension of the π system then occurs along a direction that is almost perpendicular to the polarization of the lowest electronic excitation.

By far, a much more dramatic improvement is seen in **9**. Although the frontier molecular orbitals of **8** and **9** look very similar and are in both cases mostly confined on the central BODIPY core, the transition densities extend significantly over the external phenyl rings in **9** (Figure 3), which explains the largest oscillator strength computed for that compound. This effect arises from multi-configurational mixing of the HOMO–LUMO excitation with electronic configurations involving deeper molecular orbitals with large weights on the outer phenyl rings.

Representations of the HOMO and LUMO of the compounds are available in Figure S9 in the Supporting Information.

Solvatochromism

Solvent-dependent spectral shifts are often analyzed in terms of a single parameter (i.e., by using a global single-parameter scale or one describing only nonspecific solvent effects arising from the solvent acting as a dielectric continuum). However, empirical single-parameter solvent scales

regularly appear to be unsuitable because that specific single parameter is so dependent on the particular probe used to construct the single-parameter scale concerned that it fails to predict the behavior of other solutes with considerably different properties from those of the probe. A multi-parameter approach is often preferable and has been applied successfully to various physicochemical parameters.[4]

The solvent effect can be split into two different types of contributions, namely specific interactions (i.e., described as localized donor–acceptor interactions involving specific orbitals or acid–base interactions involving hydrogen bonding) and nonspecific interactions (i.e., those arising from the solvent acting as a dielectric continuum).

The solvent effect on the physicochemical observable y can be expressed by the multi-linear Equation (2a):

$$y = y_0 + a\,A + b\,B + c\,C + d\,D \tag{2a}$$

in which y_0 denotes the physicochemical property of interest in the gas phase; a, b, c, and d are adjustable coefficients that reflect the sensitivity of the physicochemical property y in a given solvent to the various {A, B, C, D} solvent parameters. The physicochemical observables y analyzed in this paper are the absorption maxima $\bar{\nu}_{abs} = 1/\lambda_{abs}$(max), the emission maxima $\bar{\nu}_{em} = 1/\lambda_{em}$(max) and the Stokes shifts $\Delta\bar{\nu} = \bar{\nu}_{abs} - \bar{\nu}_{em}$ (all in cm^{-1}).

In the literature there are several solvent scales reported to describe the solvent dependence of y. Kamlet and Taft[27] proposed the α, β, and π^* parameters to characterize, respectively, the acidity, the basicity, and the polarity/polarizability of a solvent [Eq. (2b)].

$$y = y_0 + a_\alpha\,\alpha + b_\beta\,\beta + c_{\pi^*}\,\pi^* \quad (\text{Kamlet} - \text{Taft}) \tag{2b}$$

Recently, Catalán proposed a generalized treatment of the solvent effect based on a set of four empirical, mutually independent solvent scales.[28] The dipolarity, polarizability, acidity, and basicity of a certain solvent are characterized by the parameters SdP,[28] SP,[29] SA,[30,31] and SB,[32] respectively [Eq. (2c)].

$$y = y_0 + a_{SA}\,SA + b_{SB}\,SB + c_{SP}\,SP + d_{SdP}\,SdP \quad (\text{Catalán}) \tag{2c}$$

The Kamlet–Taft solvatochromic {α, β, π^*} parameters are taken from Ref. [33], whereas the Catalán SA and SB parameter values come from Refs [30–32]. The Catalán solvent polarizability parameters SP are collected from Ref. [29]. The new SdP solvent dipolarity parameters can be found in Ref. [28].

Compiled in Table 8 are the estimated regression coefficients y_0, a_{SA}, b_{SB}, c_{SP}, d_{SdP} (Catalán) and their respective standard errors, and the correlation coefficients (r) for the multiple linear regression analyses of the maxima of absorption ($\bar{\nu}_{abs}$) and fluorescence emission ($\bar{\nu}_{em}$) and the Stokes shift $\Delta\bar{\nu}$ of **1**–**3** according to Equation (2c) for the solvents of Tables 2–4.

Table 8. Estimated coefficients (y_0, a, b, c, d; in cm^{-1}) and correlation coefficient (r) for the multiple linear regression analysis of the absorption ($\bar{\nu}_{abs}$) and fluorescence emission maxima ($\bar{\nu}_{em}$), and the Stokes shift ($\Delta\bar{\nu}$) of **1–3** as a function of the Catalán {SA, SB, SP, SdP} solvent scales for the 20 solvents listed in Tables 2–4.

Compound		y_0	a_{SA}	b_{SB}	c_{SP}	d_{SdP}	r
1	$\bar{\nu}_{abs}$	20238 ± 105	-199 ± 58	14 ± 35	-1223 ± 141	110 ± 26	0.932
	$\bar{\nu}_{em}$	19631 ± 86	-19 ± 47	-36 ± 29	-1254 ± 115	81 ± 22	0.953
	$\Delta\bar{\nu}$	606 ± 114	-180 ± 63	50 ± 38	31 ± 154	29 ± 29	0.619
2	$\bar{\nu}_{abs}$	18928 ± 121	-177 ± 67	20 ± 40	-1139 ± 162	204 ± 30	0.935
	$\bar{\nu}_{em}$	18325 ± 91	-60 ± 50	-1 ± 31	-904 ± 122	39 ± 23	0.900
	$\Delta\bar{\nu}$	603 ± 130	-117 ± 72	20 ± 43	-235 ± 174	165 ± 33	0.816
3	$\bar{\nu}_{abs}$	18129 ± 107	-128 ± 59	1 ± 36	-1439 ± 144	148 ± 27	0.952
	$\bar{\nu}_{em}$	17660 ± 106	-12 ± 59	-28 ± 36	-1239 ± 142	46 ± 27	0.926
	$\Delta\bar{\nu}$	469 ± 130	-115 ± 72	28 ± 43	-200 ± 174	102 ± 33	0.683

Use of the Catalán solvent parameter set {SA, SB, SP, SdP} [Eq. (2c)], for which solvent (di)polarity and polarizability effects are split, gives excellent fits to $\bar{\nu}_{abs}$ (0.932 for **1**, 0.935 for **2**, and 0.952 for **3**). To visualize the goodness-of-fit of $\bar{\nu}_{abs}$ as a function of the Catalán solvent parameters {SA, SB, SP, SdP}, we plotted the $\bar{\nu}_{abs}$ values calculated, according to Equation (2c), by using the estimated values of y_0, a_{SA}, b_{SB}, c_{SP}, d_{SdP} versus the corresponding experimental $\bar{\nu}_{abs}$ values for dyes **1–3** (Figures S5a, S6a, and S7a in the Supporting Information). The analyses of the $\bar{\nu}_{abs}$ data of **1–3** according to Kamlet–Taft [Eq. (2b)] using the {α, β, π^*} solvent scales showed poor fits, as assessed by the values of r (0.315 for **1**, 0.486 for **2**, 0.324 for **3**) and the large standard errors on the estimated {a_α, b_β, c_{π^*}} coefficients as quality-of-fit criteria (Table S1 in the Supporting Information).

Excellent fits were found for the multilinear analyses of the $\bar{\nu}_{em}$ data of **1–3** according to Equation (2c) (r values were 0.953 for **1**, 0.900 for **2**, and 0.926 for **3**). The plots of $\bar{\nu}_{em}$ were calculated, according to Equation (2c), by using the estimated values of y_0, a_{SA}, b_{SB}, c_{SP}, d_{SdP} versus the corresponding experimental $\bar{\nu}_{em}$ values of **1–3** are shown in Figure S5b, S6b, and S7b (Supporting Information). Contrary to the superb results obtained by using the Catalán solvent scales, the $\bar{\nu}_{em}$ data of **1–3** could not be described adequately by the Kamlet–Taft {α, β, π^*} solvent parameters [Eq. (2b)], as judged by the low r values (0.317 for **1**, 0.325 for **2**, 0.369 for **3**) and the large standard errors on the estimated {a_α, b_β, c_{π^*}} coefficients (Table S1 in the Supporting Information).

It is remarkable that the small solvent-dependent shifts (all $\bar{\nu}_{abs}$ measured lie within $\tilde{\nu}=264\ cm^{-1}$ for **1**, $\tilde{\nu}=299\ cm^{-1}$ for **2** and $\tilde{\nu}=354\ cm^{-1}$ for **3**; all $\bar{\nu}_{em}$ measured lie within $\tilde{\nu}=317\ cm^{-1}$ for **1**, $\tilde{\nu}=218\ cm^{-1}$ for **2**, and $\tilde{\nu}=338\ cm^{-1}$ for **3**) can be described so accurately by the Catalán solvent scales. The advantage of this new, generalized treatment of the solvent effect is that it allows one to split up the relative contributions of dipolarity, polarizability, acidity, and basicity of the medium. Hence, it is informative to determine which solvent parameter is primarily responsible for the slight solvatochromic shifts of $\bar{\nu}_{abs}$ and $\bar{\nu}_{em}$ of **1–3**. It must be noted that in the Kamlet–Taft approach, the solvent scale π^* combines solvent (di)polarity and polarizability effects, and hence, this methodology can never be used to disentangle solvent polarizability and (di)polarity effects.

The large (negative) estimated c_{SP} values compared to the {a_{SA}, b_{SB}, d_{SdP}} estimates in the analysis of $\bar{\nu}_{abs}$ of **1–3** according to Equation (2c) and the relatively large standard errors on a_{SA}, b_{SB}, and d_{SdP} in comparison to those on c_{SP} (Table 8) indicate that the small change of $\bar{\nu}_{abs}$ may reflect principally a minor change in polarizability of the environment of the chromophore. Indeed, the multilinear fit according to Equation (2c) in which solvent polarizability is disregarded (i.e., with {SA, SB, SdP} as independent variables) is very poor ($r=0.451$ for **1**, 0.677 for **2**, and 0.525 for **3**), signifying that solvent polarizability is of the utmost importance. The analyses according to Equation (2c) with three independent variables including SP and SdP (namely {SA, SP, SdP}, {SB, SP, SdP}) always gave good fits ($0.874<r<0.952$), implying that the absorption maxima are hardly influenced by the acidity and basicity of the medium. The analyses which disregarded solvent dipolarity (i.e., Equation (2c) with {SA, SB, SP} as independent variables) were somewhat less acceptable ($r=0.846$ for **1**, 0.706 for **2**, 0.847 for **3**). All these analyses point to solvent polarizability as the major parameter determining the position of the absorption maxima. However, especially for **2**, dipolarity of the medium cannot be disregarded. This is corroborated by the linear regression of $\bar{\nu}_{abs}$ versus SP which is the most unsatisfactory for **2** ($r=0.679$ for **2** versus 0.803 for **1** and 0.839 for **3**). Dyes **1** and **3** are symmetric and it can be assumed that the nonsymmetric dye **2** will have a somewhat larger dipole than **1** and **3**, which can explain the larger sensitivity of $\bar{\nu}_{abs}$ of **2** to solvent dipolarity.

The relatively large (negative) c_{SP} estimates and the comparatively large standard errors on a_{SA}, b_{SB}, and d_{SdP} in comparison to those on c_{SP} (Table 8) point to solvent polarizability as the major factor affecting $\bar{\nu}_{em}$ of **1–3**. The analyses of $\bar{\nu}_{em}$ according to Equation (2c) with {SA, SB, SP}, {SB, SP, SdP}, and {SA, SP, SdP}, as independent variables, all gave high-quality fits (for **1** $r=0.908$, 0.953, and 0.948, respectively; for **2** $r=0.879$, 0.890, and 0.900, respectively; for **3** $r=0.911$, 0.926, and 0.923, respectively). The common independent variable in all these analyses is SP (solvent polarizability). Conversely, the analysis of $\bar{\nu}_{em}$ according to Equation (2c), in which SP was disregarded, gave low r-values (0.433 for **1**, 0.399 for **2**, 0.367 for **3**). Therefore, solvent polarizability is the most crucial solvent property influencing $\bar{\nu}_{em}$. Additional evidence that the position of $\bar{\nu}_{em}$ is controlled largely by solvent polarizability comes from the linear regressions of $\bar{\nu}_{em}$ versus SP ($r=0.907$ for **1**, 0.872 for **2**, 0.909 for **3**). In these linear regressions, the lowest r values are found for **2**, implying that solvent polarizability alone does not determine the position of $\bar{\nu}_{em}$. The fact that solvent polarizability is the principal factor affecting $\bar{\nu}_{abs}$ and

$\bar{\nu}_{em}$ of **1–3** can explain the failure of the Kamlet–Taft approach because solvent polarizability is not treated as a separate parameter in this methodology.

The substandard fits of the small Stokes shift $\Delta\bar{\nu}$ of **1–3** as a function of the solvent parameters {SA, SB, SP, SdP}—as substantiated by rather low *r* values (0.619 for **1**, 0.816 for **2**, and 0.684 for **3**)—are no surprise because the only solvent parameter that really matters (i.e., polarizability) has an identical effect on $\bar{\nu}_{abs}$ and $\bar{\nu}_{em}$ and hence will not affect $\Delta\bar{\nu}$.

Conclusions

We have demonstrated that the combination of nucleophilic aromatic substitution of 3,5-dichloro-4,4-difluoro-8-(4-tolyl)-4-bora-3*a*,4*a*-diaza-*s*-indacene with *o*-bromophenol, followed by palladium catalyzed benzofuran ring formation, is a powerful and facile method for the formation of BODIPY dyes with bathochromically shifted visible absorption and fluorescence spectra with considerably higher $\varepsilon(\lambda)$, *f*, and Φ_f values. Dyes **1**, **2**, and **3** have increasingly restricted conformational flexibility. Their UV/Vis absorption and fluorescence emission spectra have been determined as a function of solvent. These BODIPY derivatives show small Stokes shifts and narrow absorption and emission bands. The small solvent-dependent shifts of the absorption and emission bands of **1–3** are primarily determined by solvent polarizability. The absorption and emission maxima of **2** are shifted to the red by ≈ 30 nm in comparison to the unconstrained structure **1**. The most rigid structure **3** displays an additional bathochromic shift in both the absorption and emission spectra of ≈ 30 nm compared to **2**. These results are also supported by quantum chemical calculations which showed that the increase of conformational constraints leads to larger bathochromic shifts. The crystal structures of the three dyes have been determined and show an increasing planarity of the chromophore in line with a reduction of the conformational flexibility.

Experimental Section

The synthetic route, materials and solvents used and the experimental procedures for 1) the spectroscopic measurements, 2) the crystal structure determinations, and 3) the quantum chemical calculations can be found in the Supporting Information.

CCDC 755091 (**1**), 755092 (**2**), and 755093 (**3**) contain the supplementary crystallographic data for this paper. These data can be obtained free of charge from The Cambridge Crystallographic Data Centre at www.ccdc.cam.ac.uk/data_request/cif.

Acknowledgements

[1] A. Treibs, F.-H. Kreuzer, *Liebigs Ann. Chem.* **1968**, *718*, 208–223.

[2] a) A. Loudet, K. Burgess, *Chem. Rev.* **2007**, *107*, 4891–4932; b) G. Ulrich, R. Ziessel, A. Harriman, *Angew. Chem.* **2008**, *120*, 1202–1219; *Angew. Chem. Int. Ed.* **2008**, *47*, 1184–1201.

[3] R. P. Haugland, *The Handbook. A Guide to Fluorescent Probes and Labeling Technologies*, 10th ed., Invitrogen, Eugene, OR, **2005**.

[4] B. Valeur, *Molecular Fluorescence. Principles and Applications*, Wiley-VCH, Weinheim, Germany, **2002**.

[5] a) L. H. Thoresen, H. Kim, M. B. Welch, A. Burghart, K. Burgess, *Synlett* **1998**, 1276–1278; b) A. Burghart, H. Kim, M. B. Welch, L. H. Thoresen, J. Reibenspies, K. Burgess, F. Bergström, L. B.-Å. Johansson, *J. Org. Chem.* **1999**, *64*, 7813–7819.

[6] T. Rohand, W. Qin, N. Boens, W. Dehaen, *Eur. J. Org. Chem.* **2006**, 4658–4663.

[7] R. Rurack, M. Kollmannsberger, J. Daub, *New J. Chem.* **2001**, *25*, 289–292.

[8] Z. Dost, S. Atilgan, E. U. Akkaya, *Tetrahedron* **2006**, *62*, 8484–8488.

[9] V. Leen, E. Braeken, K. Luckermans, C. Jackers, M. Van der Auweraer, N. Boens and W. Dehaen, *Chem. Commun.* **2009**, 4515–4517.

[10] J. Chen, J. A. Burghart, A. Derecskei-Kovacs, K. Burgess, *J. Org. Chem.* **2000**, *65*, 2900–2906.

[11] a) M. Wada, S. Ito, H. Uno, T. Murashima, N. Ono, T. Urano, Y. Urano, *Tetrahedron Lett.* **2001**, *42*, 6711–6713; b) Z. Shen, H. Röhr, K. Rurack, H. Uno, M. Spieles, B. Schulz, G. Reck, N. Ono, *Chem. Eur. J.* **2004**, *10*, 4853–4871.

[12] S. Goeb, R. Ziessel, *Org. Lett.* **2007**, *9*, 737–740.

[13] K. Umezawa, Y. Nakamura, H. Makino, D. Citterio, K. Suzuki, *J. Am. Chem. Soc.* **2008**, *130*, 1550–1551.

[14] K. Umezawa, A. Matsui, Y. Nakamura, D. Citterio, K. Suzuki, *Chem. Eur. J.* **2009**, *15*, 1096–1106.

[15] A. B. Descalzo, H.-J. Xu, Z.-L. Xue, K. Hoffmann, Z. Shen, M. G. Weller, X.-Z. You, K. Rurack, *Org. Lett.* **2008**, *10*, 1581–1584.

[16] Y.-W. Wang, A. B. Descalzo, Z. Shen, X.-Z. You, K. Rurack, *Chem. Eur. J.* **2010**, *16*, 2887–2903.

[17] M. Baruah, W. Qin, N. Basarić, W. M. De Borggraeve, N. Boens, *J. Org. Chem.* **2005**, *70*, 4152–4157.

[18] M. Baruah, W. Qin, R. A. L. Vallée, D. Beljonne, T. Rohand, W. Dehaen, N. Boens, *Org. Lett.* **2005**, *7*, 4377–4380.

[19] T. Rohand, M. Baruah, W. Qin, N. Boens, W. Dehaen, *Chem. Commun.* **2006**, 266–268.

[20] T. Rohand, J. Lycoops, S. Smout, E. Braeken, M. Sliwa, M. Van der Auweraer, W. Dehaen, W. M. De Borggraeve, N. Boens, *Photochem. Photobiol. Sci.* **2007**, *6*, 1061–1066.

[21] C. Thivierge, R. Bandichhor, K. Burgess, *Org. Lett.* **2007**, *9*, 2135–2138.

[22] G. Zeni, R. Larock, *Chem. Rev.* **2006**, *106*, 4644–4680.

[23] The Cambridge Structural Database: a quarter of a million crystal structures and rising. F. H. Allen, *Acta Crystallogr. Sect. B* **2002**, *58*, 380–388 [DOI: 10.1107/S0108768102003890].

[24] The following represents a non-exhaustive list of BODIPY papers with spectroscopic/photophysical data; a) E. Vos de Wael, J. A. Pardoen, J. A. van Koeveringe, J. Lugtenburg, *Recl. Trav. Chim. Pays-Bas* **1977**, *96*, 306–309; b) T. López Arbeloa, F. López Arbeloa, I. López Arbeloa, I. García-Moreno, A. Costela, R. Sastre, F. Amat-Guerri, *Chem. Phys. Lett.* **1999**, *299*, 315–321; c) A. Costela, I. García-Moreno, C. Gomez, R. C. Sastre, F. Amat-Guerri, M. Liras, F. López Arbeloa, J. Bañuelos Prieto, I. López Arbeloa, *J. Phys. Chem. A* **2002**, *106*, 7736–7742; d) F. López Arbeloa, J. Bañuelos

Prieto, V. Martínez Martínez, T. Arbeloa López, I. López Arbeloa, *ChemPhysChem* **2004**, *5*, 1762–1771; e) J. Bañuelos Prieto, F. López Arbeloa, V. Martínez Martínez, T. Arbeloa López, F. Amat-Guerri, M. Liras, I. López Arbeloa, *Chem. Phys. Lett.* **2004**, *385*, 29–35; f) W. Qin, M. Baruah, M. Van der Auweraer, F. C. De Schryver, N. Boens, *J. Phys. Chem. A* **2005**, *109*, 7371–7384; g) W. Qin, T. Rohand, M. Baruah, A. Stefan, M. Van der Auweraer, W. Dehaen, N. Boens, *Chem. Phys. Lett.* **2006**, *420*, 562–568; h) Z. Li, R. Bittman, *J. Org. Chem.* **2007**, *72*, 8376–8382; i) Z. Ekmekci, M. D. Yilmaz, E. U. Akkaya, *Org. Lett.* **2008**, *10*, 461–464; j) L. Li, J. Han, B. Nguyen, K. Burgess, *J. Org. Chem.* **2008**, *73*, 1963–1970; k) E. Fron, E. Coutino-Gonzalez, L. Pandey, M. Sliwa, M. Van der Auweraer, F. De Schryver, J. Thomas, Z. Dong, V. Leen, M. Smet, W. Dehaen, T. Vosch, *New J. Chem.* **2009**, *33*, 1490–1496.

[25] S. E. Braslavsky, *Pure Appl. Chem.* **2007**, *79*, 293–465.

[26] R. A. L. Vallée, M. Van der Auweraer, F. C. De Schryver, D. Beljonne, M. Orrit, *ChemPhysChem* **2005**, *6*, 81–91.

[27] a) M. J. Kamlet, R. W. Taft, *J. Am. Chem. Soc.* **1976**, *98*, 377–383; b) M. J. Kamlet, J. L. M. Abboud, R. W. Taft, *J. Am. Chem. Soc.* **1977**, *99*, 6027–6038.

[28] J. Catalán, *J. Phys. Chem. B* **2009**, *113*, 5951–5960.

[29] J. Catalán, H. Hopf, *Eur. J. Org. Chem.* **2004**, 4694–4702.

[30] J. Catalán in *Handbook of Solvents*, (Ed.: G. Wypych), ChemTec Publishing, Toronto, **2001**, pp. 583–616.

[31] J. Catalán, C. Díaz, *Liebigs Ann.* **1997**, 1941–1949.

[32] J. Catalán, C. Díaz, V. López, P. Pérez, J. L. G. de Paz, J. G. Rodriguez, *Liebigs Ann.* **1996**, 1785–1794.

[33] Y. Marcus, *Chem. Soc. Rev.* **1993**, *22*, 409–416.